Nuclear pore complexes undergo Nup221 exchange during blood stage asexual replication of *Plasmodium* parasites.

Authors:

James Blauwkamp[1]*, Sushma V Ambekar[2]*, Tahir Hussain[2], Gunnar R Mair[2,3#], Josh R. Beck[2#], Sabrina Absalon[1#]

Affiliations:

[1]Indiana University School of Medicine, Department of Pharmacology and Toxicology

[2]Iowa State University, Department of Biomedical Sciences

[3]School of Biological Sciences, Queen's University Belfast

*These authors contributed equally

[#]Co-corresponding Authors

Abstract

Plasmodium parasites, which are the causative agents of malaria, undergo closed mitosis without breakdown of the nuclear envelope. Unlike the closed mitosis in yeast, *P. berghei* parasites undergo multiple rounds of asynchronous nuclear divisions in a shared cytoplasm result in a multinucleated (8-24) organism prior to formation of daughter cells within an infected red blood cell. During this replication process, intact nuclear pore complexes (NPCs) and their component nucleoporins are likely to play critical roles in parasite growth, facilitating selective bi-directional nucleocytoplasmic transport and genome organization. Here we utilize ultrastructure expansion microscopy (U-ExM) to investigate *P. berghei* Nup138, Nup221, and Nup313 at the single nucleus level throughout the 24 hour blood-stage replication cycle. Our findings reveal that these Nups are evenly distributed around the nuclei and organized in a rosette structure previously undescribed around the centriolar plaque, which is responsible for intranuclear microtubule nucleation during mitosis. We also detect an increased number of NPCs compared with previously reported, highlighting the power of U-ExM. By adapting the recombination-induced tag exchange (RITE) system to *P. berghei*, we provide evidence of NPC maintenance, demonstrating Nup221 turnover during parasite asexual replication. Our data shed light on the distribution of NPCs and their homeostasis during the blood-stage replication of *P. berghei* parasites. Further studies into the nuclear surface of these parasites will allow for a better understanding of parasites nuclear mechanics and organization.

39 **Introduction:**

40 The survival and growth of eukaryotic organisms relies on the movement of
41 macromolecules between the membrane bound nucleus and the cytosol. This nuclear-cytosolic
42 transport is facilitated by nuclear pore complexes (NPCs) that are embedded into the nuclear
43 envelope. Apart from being a channel for selective bidirectional nucleocytoplasmic transport, the
44 NPC plays a key role in chromatin organization, gene regulation, DNA repair, and maintenance of
45 epigenetic memory in many eukaryotes [1]. Typically, these NPCs are composed of multiple copies
46 of more than 30 different nucleoporins (Nups) per NPC, with eukaryotic NPCs containing around
47 1000 proteins total [1-5]. Nups are widely conserved in most eukaryotes, including yeasts,
48 humans, and various plant species, and have also been identified in parasitic protozoa such as
49 *Trypanosoma brucei* and *Toxoplasma gondii* [6, 7]. Nups are separated into two distinct
50 categories; structural Nups that form the pore and the intrinsically disordered phenylalanine-
51 glycine repeat (FG) Nups which regulate nucleocytoplasmic transport (Figure 1a) [8, 9].
52 Structurally, the NPCs establish an inner channel called the inner ring, flanked by the outer rings
53 on the cytosolic and nuclear side of the NPC. After the inner channel is constructed the
54 cytoplasmic filament and the nuclear basket Nups attach to their appropriate side of the pore [8,
55 9]. The FG Nups, characterized by their FG repeats, occupy the space inside the inner ring and
56 interact with the cargo to facilitate nuclear-cytosolic transport [8-10].

57 One of the most extensively studied organisms with respect to the dynamics and
58 structural aspects of nuclear pore complexes is budding yeast. *Saccharomyces cerevisiae*
59 undergoes closed mitosis during which the nuclear envelope remains intact during karyokinesis.
60 In contrast to open mitosis, where NPC removal during prophase leads to nuclear envelope

61 breakdown, in closed mitosis it has been hypothesized that specific regions of nuclear pore/
62 complex disassembly cause small breaks in the nuclear envelope, facilitating nuclear envelope
63 fission and formation of two new nuclei [11, 12]. Like budding yeast, the parasites of the
64 *Plasmodium* genus, the causative agent of malaria, undergo a specialized form of closed mitosis.
65 In these parasites, multiple rounds of asynchronous nuclear division in a shared cytoplasm leads
66 to a multinucleated single-celled parasite [13]. While many Nups are conserved through
67 eukaryotes, *Plasmodium* Nups are very divergent, which makes their identification by
68 bioinformatics challenging. In a 2010 study aiming to identify Nups of different eukaryotes, only
69 two Nups were identified in *P. berghei* compared to 19 identified Nups in over 50 different
70 organisms [14]. Eleven Nups are currently known in the rodent malaria model *P. berghei*; Sec13.
71 Five FG Nups, and five novel Nups identified using Nup313 as bait in proximal labeling assays
72 (Figure 1a) [15-17]. Interestingly, only one of these proteins presents established structural
73 features of eukaryotic Nups [8].

74 The limited understanding of essential components of nuclear pore complexes in
75 *Plasmodium* is attributed to the absence of protein homology for Nup identification in
76 *Plasmodium* and the lack of suitable tools to investigate the dynamics of NPCs within relatively
77 small nuclei (a micrometer). While conventional fluorescence and electron microscopy
78 techniques have provided valuable insights into the perinuclear localization of identified Nups in
79 *Plasmodium* parasites, these approaches suffer from low resolution and the significant financial
80 and time investments required for electron microscopy [8, 11, 15, 18-22]. These challenges in
81 comprehending the dynamics and distribution of nuclear pore complexes (NPCs) in *Plasmodium*
82 parasites have spurred the exploration of innovative microscopy techniques to overcome these

83 limitations and gain deeper insights into these vital components. The adaptation of Ultrastructure
84 Expansion Microscopy (U-ExM) to work with parasites now allows for super-resolution imaging
85 of parasites in a cost-effective and high-throughput manner [23-26]. U-ExM achieves isotropic
86 expansion of biological samples, increasing their size up to 4.5 times by embedding denatured
87 samples into a hydrogel that expands when exposed to water. Notably, this technique has been
88 employed to achieve sub-nucleus resolution and has successfully visualized Nup313 at the
89 nuclear membrane in *P. falciparum* [23, 25].

90 In this study, we employed U-ExM to visualize individual NPCs using tagged versions of *P.*
91 *berghei* Nup138, Nup221, and Nup313. We successfully localized these Nups to the nuclear
92 envelope by employing NHS ester or BodipyFL Ceramide staining throughout the asexual life cycle
93 of the *P. berghei* parasite. Consistent with prior findings using "serial surface" imaging in focused
94 ion beam – scanning electron microscopy (FIB-SEM)[21], we observed an increase in NPC number
95 until the parasite's first mitosis, during which the NPCs were then distributed between the newly
96 developing nuclei. We proceeded to assess NPC assembly and protein turnover using the
97 Recombination Induced Tag Exchange (RITE) system marking the first time this has been
98 accomplished in *Plasmodium*. The RITE system uses a conditional, hormone activated Cre-
99 recombinase to generate permanent epitope tag switch in a target coding sequence. This method
100 has been previously utilized in human cells to observe the dynamic replacement of NPC
101 components in human neurons [27, 28].

102 Leveraging the enhanced resolution of U-ExM coupled with the RITE system, we were able
103 to monitor NPC assembly and maintenance dynamics within a single nucleus during *Plasmodium*
104 replication. In line with previous observations in mammalian cells, we found that NPCs in *P.*

105 *berghei* undergo protein maintenance after the NPCs have been produced. Remarkably, we also
106 confirmed the presence of Nup221 proteins of different ages in a single NPC by colocalization of
107 original and induced Nup221 signal. Our results expand upon existing data and showcase the new
108 insights achievable through the combination of U-ExM with genetic and biochemical systems.

109 **Results:**

110 **U-ExM visualization of Nups around the nucleus.**

111 Previous studies on NPCs in various organisms have predominantly relied on slide-based
112 immunofluorescence assays. For higher resolution, NPCs could be visualized by electron
113 microscopy, but this process is time consuming and costly. The emergence of expansion
114 microscopy in smaller organisms like yeast has significantly advanced NPC visualization and study
115 [29]. In our efforts to visualize nucleoporins (Nups) at single NPC resolution in *P. berghei*, we
116 introduced C-terminal endogenous epitope tags on three previously identified *P. berghei* FG Nups:
117 spaghetti monster Hemagglutinin (smHA) tags on Nup138 and Nup313 and a 3xHA/GFP tag on
118 Nup221 (Supplemental figure 2). In comparison to previous studies on unexpanded parasites [15,
119 17], and considering the expected size of the NPCs in yeast [29], expansion microscopy
120 successfully resolves individual NPCs around the nuclear periphery (Figure 1b). To confirm the
121 position of these Nups at the nuclear membrane, we employed different approaches, visualizing
122 the nuclear membrane using an endoplasmic reticulum (ER) antibody (PfBIP), employing
123 membrane stains such as Bodipy TR Ceramide and Bodipy FL Ceramide, and assessing membrane
124 localization through NHS Ester staining variations around the nucleus (Supplemental figure 1).
125 Among these methods, we determined that differences in NHS ester staining and high

126 concentrations of Bodipy FL Ceramide effectively delineated the nuclear envelope to confidently
127 assign the NPC signal to this structure. In summary, U-ExM allows us to observe individual NPCs
128 on the nuclear envelope.

129 ***Plasmodium berghei* produces NPCs primarily before mitosis**.

130 We next wanted to quantify the number of NPCs surrounding each nucleus during various
131 stages of the parasite's intraerythrocytic development cycle. To achieve this, we performed U-
132 ExM on parasites that exhibited a range of nuclear numbers and were stained for either
133 Nup138::smHA or Nup313::smHA. In the early stages of the parasite's life cycle, before the
134 parasites begin their mitotic phase (1n, Ring), we observed Nup138 being uniformly distributed
135 around the nucleus (Figure 2a), while the Nup313 signal is concentrated at either end of the
136 nucleus (Supplemental figure 3). At this stage, we noticed a higher number of Nup313 foci
137 (approximately 40-50 NPCs) compared to Nup138 (around 25-35 NPCs) (Figure 2b). As the
138 parasites began mitosis (1n, Trophozoite premitotic and mitotic), there was a significant 5-fold
139 increase in both Nup138 and Nup313 numbers. The parasites produce over 250 NPCs containing
140 Nup313 and over 150 NPCs containing Nup138, distributed around the single nucleus (Figure 2b).
141 As more nuclei are formed (2-4n Schizont, 5-9n Schizont, 10+n Cytokinesis), the number of NPCs
142 around each nucleus decreased. Initially, approximately 250 NPCs surrounded a single nucleus,
143 which then reduced to around 90-100 NPCs around each of the 2 or 3 nuclei. Eventually, the count
144 further decreases to approximately 25-30 NPCs around 10-12 nuclei (Figure 2b). Our data
145 suggests that NPC production peaks before mitosis and NPCs are then distributed during each
146 karyokinesis.

147 ***Plasmodium berghei* NPCs are organized around the centriolar plaque.**

148 During and after the first mitosis we observe a uniform distribution of NPCs around
149 individual nuclei, as visualized by Nup138 and Nup313 (Figure 2). Interestingly, upon the first
150 round of mitosis we detect 4-10 foci of Nup138, Nup313, and Nup221, the homolog to yeast
151 Nup100, localizing around the centriolar plaque (CP), which is the nuclear microtubule
152 organization center responsible for intranuclear microtubule nucleation (Figure 3a)[25, 30, 31].
153 Quantification of NPCs around the centriolar plaque reveals a higher count of Nup313 compared
154 to the other two FG Nups used in this study (Figure 3b). It is important to highlight that after
155 parasite cytokinesis, the centriolar plaque disassembles [25], but NPCs retain a rosette formation
156 in the vicinity of the former plaque location (Figure 3c).

157 **The RITE system reveals NPC assembly and maintenance.**

158 NPCs in yeast undergo degradation and replacement of Nups and full NPCs [32-34], and
159 that Nup replacement occurs in non-dividing human cells [27]. Therefore, in order to assess the
160 turnover of Nups in *Plasmodium*, we adapted the Recombination Induced Tag Exchange (RITE)
161 system for the first time in these parasites. The RITE system uses a constitutively expressed Cre
162 recombinase fused to the human estrogen binding domain (EBD) which retains the protein in the
163 cytoplasm by association with HSP70. Upon the addition of β-estradiol, Cre-EBD translocates to
164 the nucleus where it triggers a permanent genetic switch through a recombination event between
165 two *LoxP* flanking the initial tag, removing this tag and bringing a distinct tag into frame [28]
166 (Supplemental figure 4a). Here we tagged *P. berghei* Nup221 with a RITE system cassette, which
167 includes a 3xHA/GFP tag, a 3xMyc/RFP tag, and the two *LoxP* sites for tag switching (Figure 4a).

168 We found that adding as little as 2 nM β-estradiol resulted in a partial switch from HA to Myc tag,
169 while 200 nM β-estradiol induces sufficient relocation into the nucleus for a complete switch from
170 HA to Myc tag in as little as 2 hours, confirmed by PCR analysis (Supplemental figure 4b, c).

171 Initial immunofluorescence imaging over the course of a 16-hour period for both control
172 and 200 nM β-estradiol treated parasites showed visible tag switching by eight hours post
173 induction with β-estradiol (Supplemental figure 5a). By the end of the 16-hour period we
174 observed individual parasites (merozoites) that expressed a mixture of Nup221 tagged with GFP
175 or RFP, both in a typical polar localization. By PCR genotyping, we can detect tag exchange within
176 two hours of estrogen addition. Notably, the continued detection of Nup221-HA through 16 hours
177 post induction indicates a stable population of Nup221 persists for at least eight hours during the
178 parasite life cycle (Supplemental figure 5). To validate complete turnover of Nup221 and ensure
179 no spurious excision was occurring, samples from control and induced conditions were allowed
180 to propagate for an additional 96 hours (four parasite development cycles). While Myc-tagged
181 Nup221 was never detected in control samples, HA-tagged Nup221 was no longer detectable in
182 β-estradiol treated parasites after 96 hours. These results demonstrate that the RITE system is an
183 effective tool for monitoring Nup221 turnover in *P. berghei.* Pairing this technique with U-ExM
184 will provide better resolution for determining NPC maintenance in the parasites.

185 ***Plasmodium berghei* replaces Nups in post-mitotic NPCs.**

186 To investigate NPC assembly and maintenance during and after mitosis, we treated newly
187 invaded parasites (1N) with 200 nM β-estradiol and cultured for 20 hours. We then collected
188 processed samples for U-ExM at 0, 10, and 20 hours post induction with β-estradiol to determine

189 Nup221 presence in NPCs before mitosis occurs (10 hours post induction) and after mitosis,
190 during cytokinesis (20 hours post induction). We hypothesized that if Nup221 is being replaced in
191 the post-mitotic NPCs, we would observe a signal shift from the original HA signal (pink) to the
192 induced Myc signal (yellow), with a higher proportion of induced signal in the 20 hours post
193 induction samples.

194 At 0 hours post induction, early-stage parasites display only the original HA signal (Figure
195 4b). At 10 hours post induction, parasites mature and undergo the first rounds of mitosis resulting
196 in the formation of 2-3 nuclei. These parasites exhibit a mix of the HA and Myc signals, with 50%
197 of foci containing only HA signal, 35% of foci containing only Myc signal, and 15% of foci
198 containing both the HA and Myc signals (Figure 4b, c). The presence of co-localized HA and Myc
199 signals suggests multiple copies of Nup221 in individual NPCs. By 20 hours post induction with β-
200 estradiol the parasites have stopped producing new NPCs. At this time we found 35% of NPCs
201 contain only HA signal, while 50% of NPCs contain only Myc signal and 15% of NPCs contain both
202 HA and Myc signal (Figure 4b, c). This result suggests novel Nup221-Myc incorporation into
203 existing NPCs after the parasites have stopped producing them.

204 Subsequently, we wondered whether the Nups in the NPCs around the CP were subjected
205 to maintenance at the same rate as those around the nuclei. To test this, we specifically
206 monitored the turnover of Nup221 within the NPCs surrounding the CP. At 0 hours post induction,
207 when no CPs are visible, Nup221 is evenly distributed around the parasite nucleus. By 10 hours
208 post induction the CP is present, and now 50% of the NPCs surrounding it contained only the
209 original signal, mirroring observations around the rest of the nucleus. Around 20% of the NPCs
210 contain only the induced signal, a decrease of 15% compared to around the ones around the

211 nucleus, and 30% of the NPCs contain both the original and induced signal, an increase of 15%
212 compared to those scattered around the nucleus (Figure 4d). This suggests that the turnover of
213 the original Nup221 signal occurs at a slower pace in the NPCs surrounding the nucleus compared
214 to those scattered around it. This trend persists at 20 hours post induction, where 30% of NPCs
215 showed only the original signal, similar to what was seen around the rest of the nucleus. However,
216 45% of the NPCs contain only the induced signal (a decrease from 50%) and 25% of the NPCs
217 contain both the original and induced signal (an increase from 15%) (Figure 4d). Altogether, our
218 data indicate that proteins in the NPCs surrounding the CP exhibit greater stability than those in
219 NPCs scattered around the nucleus.

220

221 **Discussion**

222 In this study, we applied U-ExM and the RITE System to investigate the distribution and
223 homeostasis of NPCs in the asexual blood stages of the rodent malaria model, *P. berghei*. Previous
224 work on Nups in *Plasmodium* presented challenges due to both the divergent nature of the Nups
225 and the relatively small size of the parasite nucleus at approximately 1 µm. Our results
226 demonstrate the effectiveness of U-ExM in resolving individual NPCs around the parasite nucleus,
227 enabling us to address questions about their individual characteristics. Additionally, for the first
228 time we adapted the RITE system in *Plasmodium,* allowing us to dissect the mechanisms of NPC
229 maintenance. While the RITE system was employed here to monitor protein turnover by tag
230 exchange, it should also be amenable to other conditional mutagenesis strategies, providing an

231 alternative conditional excision strategy in addition to the established dimerizable Cre (DiCre)
232 system [35, 36], expanding the genetic toolkit in this important rodent malaria model.

233 This study defined the number of Nups surrounding the nucleus during the asexual life
234 cycle of *P. berghei*, unraveling a dual localization of NPCs around individual nuclei. Interestingly,
235 we observed a rosette structure around the centriolar plaque (CP) during nuclear replication and
236 this NPC organization persisted in merozoites even when the CP was no longer visible. Our
237 findings align with Ferreira et al, using CryoEM to examine microtubules in *P. falciparum* parasites,
238 revealing a similar ordered NPC structure around the CP during mitosis [37]. This circular
239 organization, previously unreported and not observed outside of *Plasmodium*, could suggest a
240 specific role of these NPCs in CP formation, duplication, maintenance, and function during
241 mitosis. For example, *S. cerevisiae* NPC protein Ndc1, a subunit of the transmembrane ring, is a
242 key protein in inserting the nuclear MTOC into the nuclear envelope [38, 39].

243 By quantifying individual Nup foci around the nuclei, we determined the number of NPCs
244 per nucleus throughout the life cycle. Our results indicate a rapid increase in NPCs just before the
245 first round of mitosis, consistent with previous observations *in P. falciparum* [21]. The higher NPC
246 count observed in our study (250 vs 60) might be attributed to greater sample numbers
247 achievable with U-ExM compared to FIB-SEM (our data was taken from 150+ nuclei from 60+ cells
248 over two biological samples) and improved NPC detection by immunostaining against the
249 endogenously tagged Nups.

250 Previous research in various cell types has shown that the composition of NPCs at specific
251 stages in the cell cycle can influence cell fate [40, 41]. In *Plasmodium* parasites it has been shown

252 that SEC13, a component of the nuclear pore complexes and the COPII coat, show a different
253 localization than FG Nups [15]. Our study delved into the heterogeneity of NPCs by examining
254 three FG-Nups: Nup138, Nup221 and Nup313. Notably, Nup313 showed a distinct localization in
255 the early ring stage of the parasite suggesting a potential specialized role during this stage of
256 development. Further investigations into the dynamic localization of different types of Nups
257 would be interesting to assess whether Nup313's temporal differential localization is unique or
258 shared with other Nups that compose the NPC.

259 Our data indicate that most NPCs contain a single version of Nup221, whether pre-mitotic
260 (Figure 4c – Nup221-HA, pink) or post-mitotic (Figure 4c – Nup221-Myc, yellow). However, some
261 NPCs exhibited both pre- and post-mitotic proteins, suggesting a gradual turnover in response to
262 protein degradation or damage (Figure 4c). These observations echoed findings using the RITE
263 system by Toyama et al., suggesting an active mechanism for NPC maintenance in mammalian
264 cells [27]. This could also point towards the octagonal rotational symmetry that has been seen in
265 other organisms [42, 43]. Interestingly, we note a slight increase in protein stability around the
266 CPs, illustrated by higher colocalization between Nup221-HA and Nup221-Myc proteins than
267 around the rest of the nucleus (Figure 4d), suggesting a higher longevity of this FG Nup in NPCs
268 rosette compared to those scattered across the nucleus.

269 With the identification of numerous Nups in the *Plasmodium* genome [15, 17], and
270 improved tools for visualizing NPCs, we are now poised to investigate the individual functions of
271 Nups. While the exact roles of specific Nups in the *Plasmodium* parasites remains unknown,
272 studies in other organisms have illuminated the involvement of FG Nups in various cellular
273 processes such as protein synthesis [44], NPC localization and composition [45, 46], as well as

274 RNA transport [6, 47]. While no studies of specific FG Nup function have been conducted in
275 *Plasmodium* parasites, deletions of Nup138 and Nup221 in genome wide screens and individual
276 knock-out attempts have shown all Nups to be essential [48-50]. Likewise, partial knockdown of
277 the Nup SEC13 in human malaria slows growth of the parasite in the blood [16], while a C-terminal
278 proline enriched sequence from SEC13 in mouse malaria models is required for parasite growth
279 [15]. Thus, it is likely that disruption of Nups can lead to growth delays and impaired cell viability
280 in malaria parasites. Our work, along with prior studies, lays the foundation for future research
281 into these divergent Nups as techniques for efficient knockdown continue to advance in malaria
282 parasites.

283 One of the hallmarks of nuclear envelope breakdown in mammalian open mitosis is the
284 disassembly of NPCs following mitotic kinase signaling [51, 52]. This disassembly is a decisive step
285 where multiple Nups are phosphorylated and sequestered to be used upon nuclear envelope
286 reassembly [53]. In contrast, *Plasmodium* parasites, like yeast, undergo closed mitosis, where the
287 nuclear envelope remains intact during nuclear division [13]. Recent work in fission yeast has
288 used confocal microscopy [11] and expansion microscopy [29] to look at the distribution and
289 dynamics of NPCs in a closed mitosis model. These studies identified NPCs at the bridge between
290 dividing nuclei before nuclear envelope fission. The authors hypothesize that through currently
291 unknown mechanisms, NPC disassembly in the bridge between dividing nuclei contributes to
292 nuclear envelope disassembly, enabling nuclear division. While we observed instances of dividing
293 nuclei with a cluster of NPCs along this bridge, further investigation is needed to explore this
294 mechanism in *Plasmodium* parasites. Identification and characterization of a cytoplasmic facing

295 Nup will allow for this hypothesis to be studied further, and potentially probe into the
296 mechanisms that determine where NPC disassembly occurs and its link to nuclear fission.

297 In conclusion, our study provides novel insights into the distribution, homeostasis, and
298 homogeneity of NPC complexes in *P. berghei* throughout the asexual life cycle. Understanding the
299 dynamics of these essential components is crucial, as NPCs play a vital role in parasite survival.
300 The methodologies employed here pave the way for further in-depth investigations into the
301 functions of these divergent complexes, facilitating a comprehensive understanding of their role
302 in *Plasmodium* biology. This study sets the stage for future investigations into the diverse Nups in
303 the *Plasmodium* genome and their individual functions. Disruption of Nups, whether structural
304 or FG Nups, likely impacts cell growth and viability in malaria parasites, as observed in related
305 studies. As techniques for knockdown efficiency improvement continue to evolve, exploring the
306 specific functions of Nups in *Plasmodium* is imminent.

307

308

309

310

311

312

313

314

315

316 **Figures:**

a.

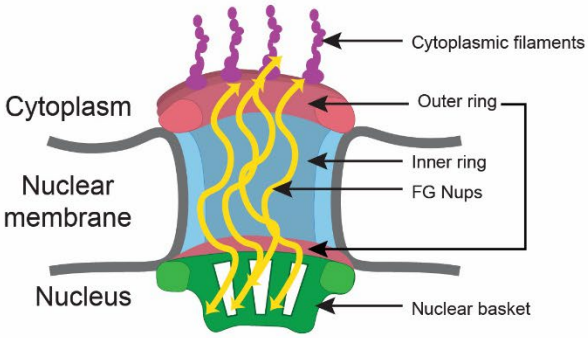

	Yeast		*P. falciparum*		*P. berghei*	
Cytoplasmic filaments	Nup159	Nup42				
Outer ring	Nup133 Nup120 Nup145C Nup85	Nup84 Seh1 Sec13	Sec13		Sec13	
Inner ring	Nup192 Nup188	Nup170 Nup157				
FG Nups	Nup145N Nup116 Nup100* NSP1	Nup57 Nup49 Nup53 Nup59	Nup116 Nup138 Nup205 Nup221*	Nup313 Nup637**	Nup138 Nup205 Nup221*	Nup313 Nup637
Nuclear basket	Nup60 Nup1 Nup2	Mlp1 Mlp2				

Magenta Nups indicate Nups used for this study.
*Homologs, **Predicted Nup

b.

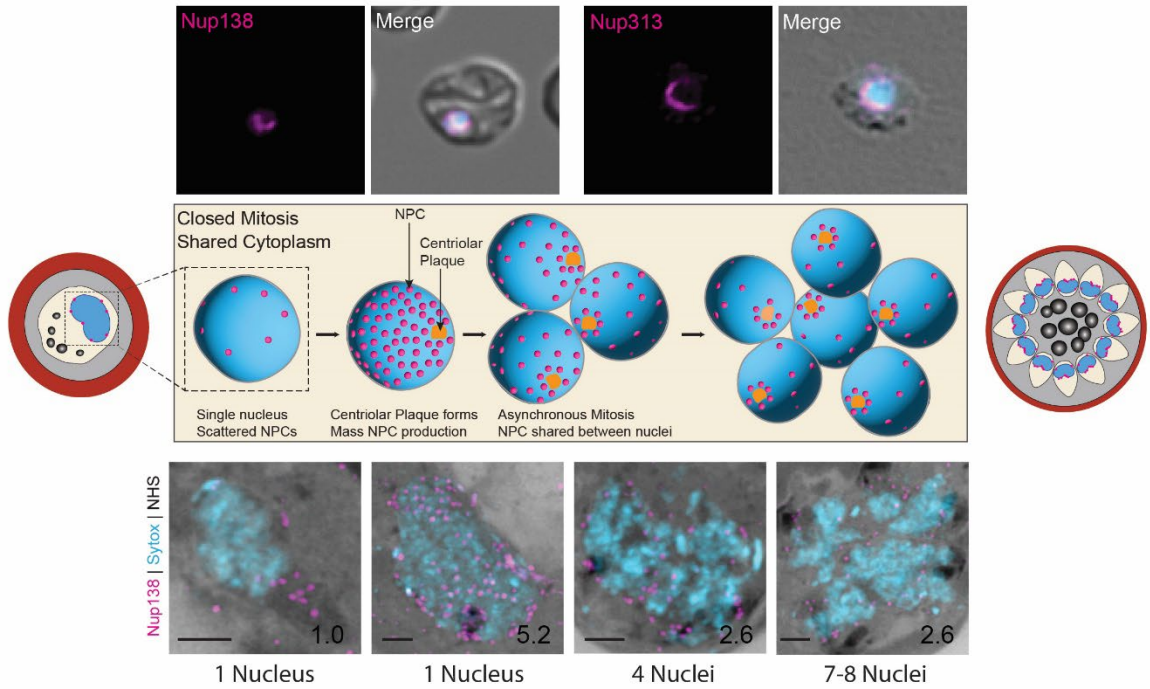

317

318 **Figure 1: Divergent *P. berghei* NPCs can be analyzed by ultrastructure expansion microscopy (U-**
319 **ExM)**. **a.** Schematic representation and table of known nucleoporins (Nups) in yeast, *P.*
320 *falciparum*, and *P. berghei*. Nups highlighted in magenta indicate Nups visualized in this study,
321 Nups marked with an asterisk represent homologs, Nup637 predicted Nup. **b.** Schematic
322 representation of the *P. berghei* life cycle inside of host red blood cells, showing NPC distribution.
323 Parasites begin with a single nucleus that undergoes mitosis midway through the life cycle.
324 Multiple rounds of asynchronous mitosis lead to a multinucleated parasite with a single

325 cytoplasm before a shared cytokinetic event produces individual parasites. Also shown are
326 comparisons between unexpanded and U-ExM images of Nup138-smHA and Nup313-smHA
327 (magenta) through the life cycle showing differences in these microscopy techniques. Under the
328 U-ExM images lists the number of nuclei in the parasites shown. Scale bars 2 µm, number on
329 images indicates image depth in µm.

330

331

332

333

334

335

336

337

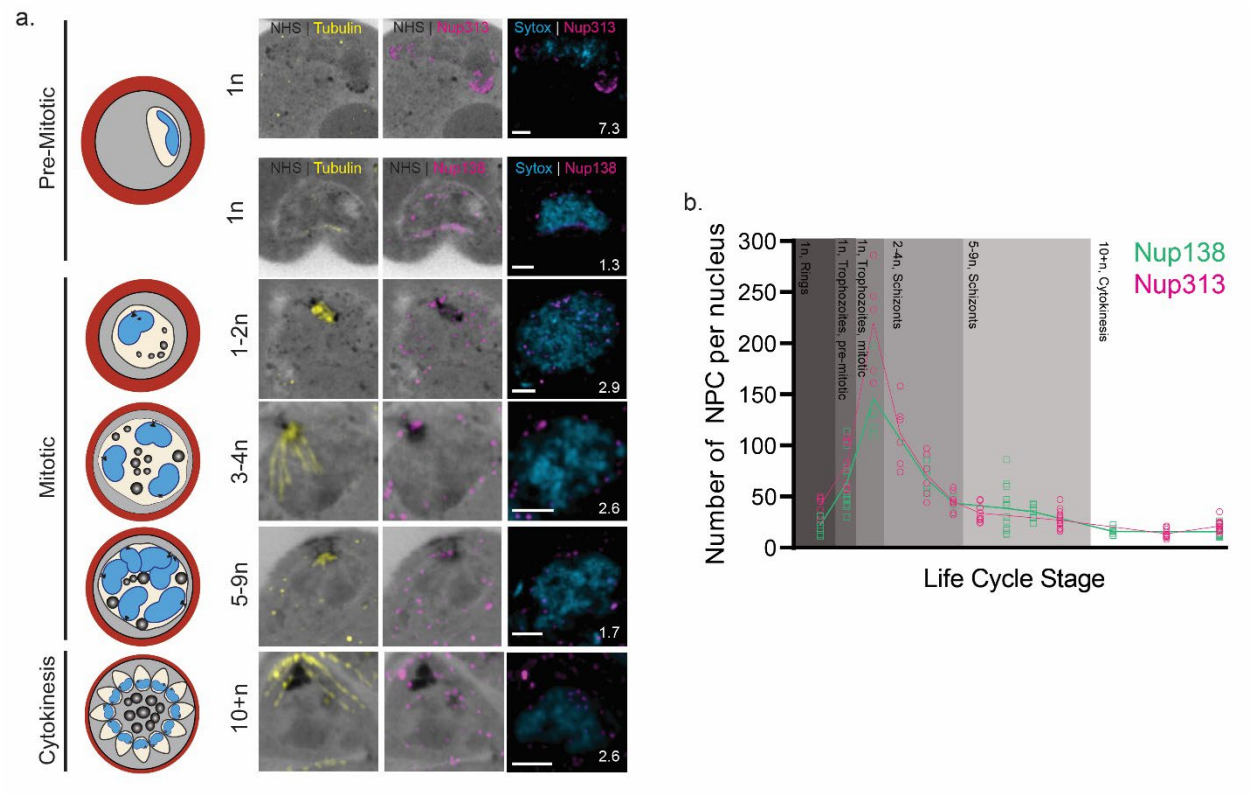

Figure 2: *P. berghei* produces NPCs until mitosis, distributing them among replicated nuclei.

a. U-ExM images showing Nup313-smHA at early stages and Nup138-smHA through the life cycle of *P. berghei*. Microtubules shown in yellow, Nup138-smHA shown in magenta, DNA shown in blue, and protein density shown in grayscale. Scale bars 2 µm, image depth in µm indicated. **b.** Number of NPCs per nucleus through the *P. berghei* life cycle calculated by counting Nup138-smHA and Nup313 signal. Green indicates Nup138 signal and magenta indicates Nup313-smHA signal.

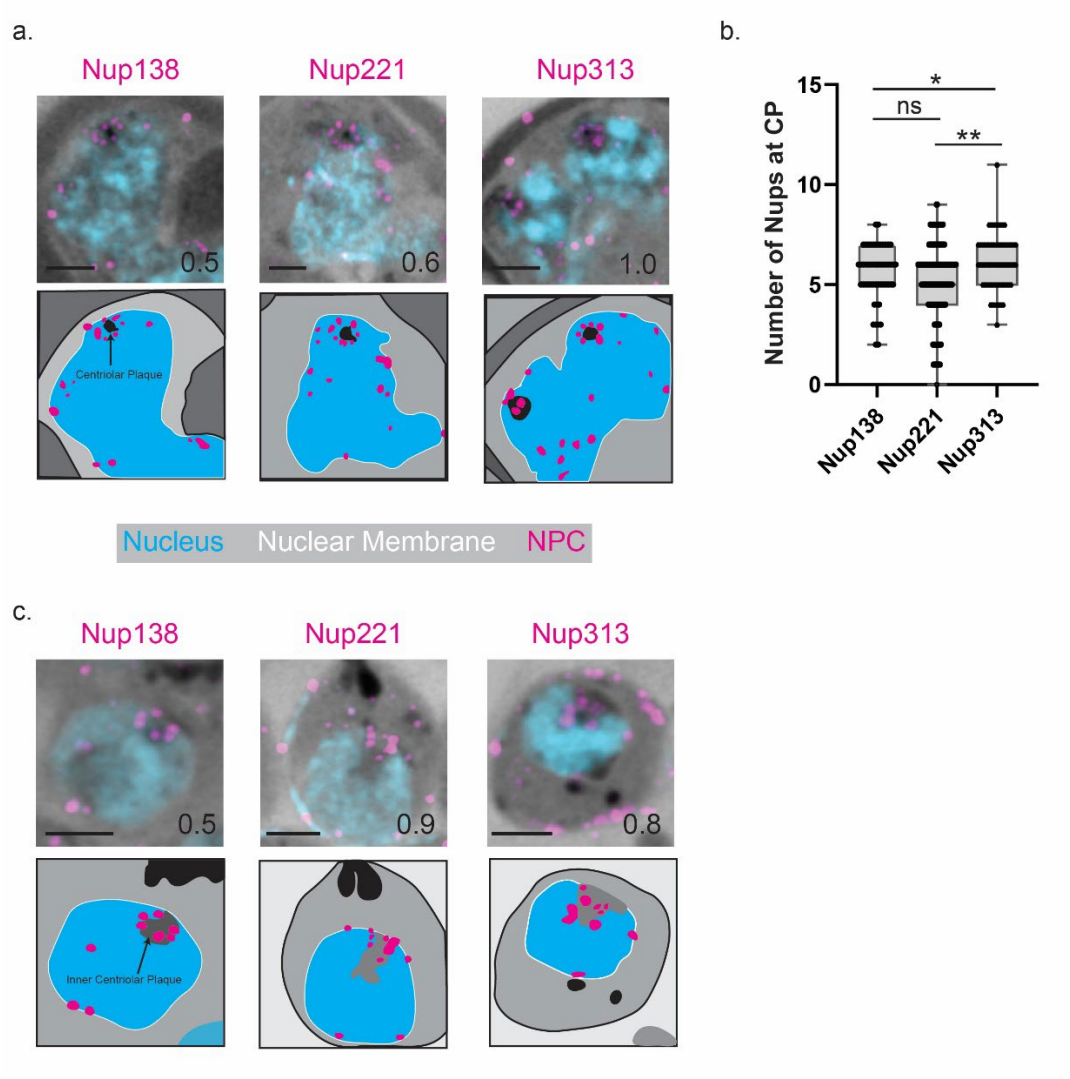

346

347 **Figure 3: P. berghei NPCs organize around the centriolar plaque (CP) during and after mitosis.**
348 **a.** Representative images of mitotic nuclei containing CPs (indicated by black staining of NHS
349 ester) and the organization of three respective FG Nups around the CP. Nups are shown in
350 magenta, DNA is shown in blue, protein density is shown in grayscale. **b.** Quantitation of Nups
351 around the CPs in Nup138-smHA, Nup221-3xHA/GFP, and Nup313-smHA stained NPCs. *
352 indicates P-value > 0.05, ** indicates P-value >0.005. **c.** Representative images of post-mitotic CPs
353 and the organization of three respective FG Nups around where the inner CP disassembles. Nups
354 are shown in magenta, DNA is shown in blue, protein density is shown in grayscale Scale bars 2
355 µm, image depth in µm indicated on the image.

356

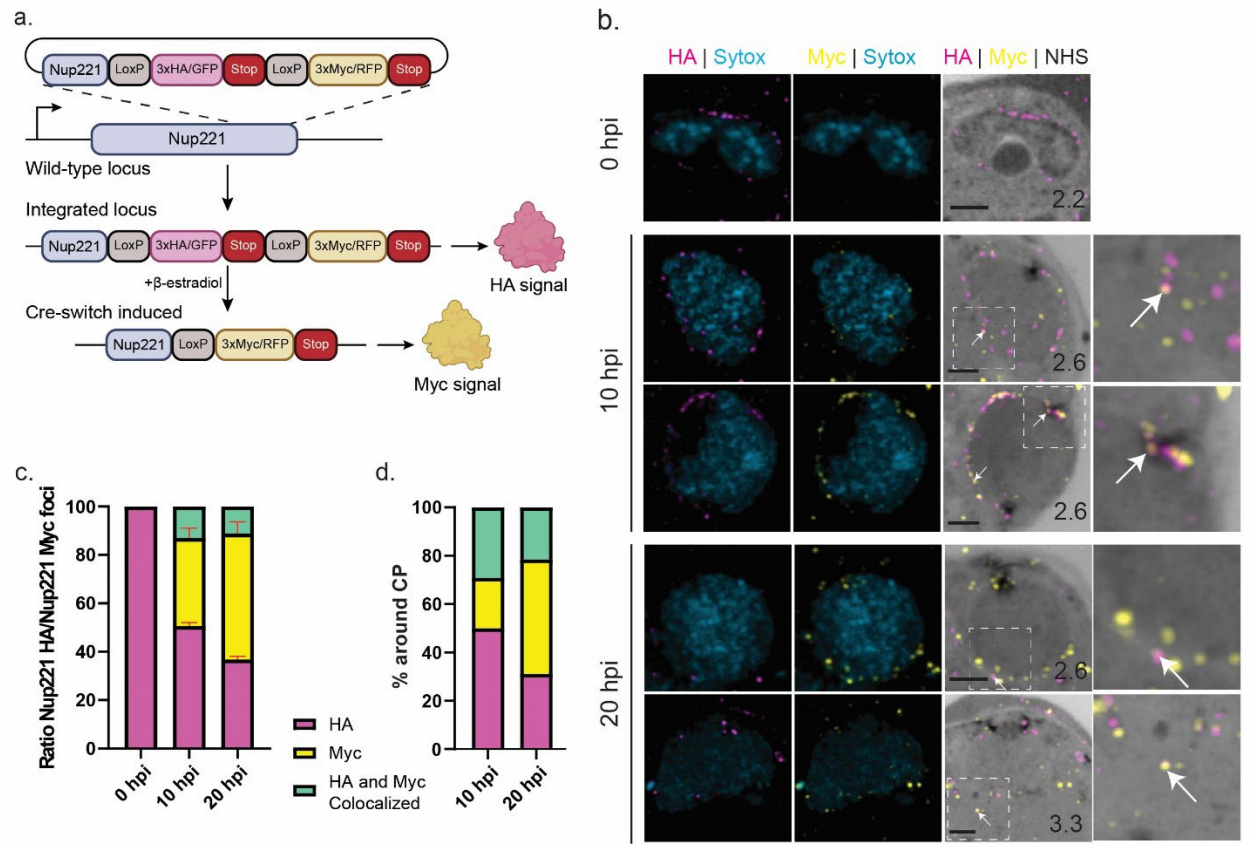

Figure 4: *P. berghei* replaces Nups in post-first mitotic NPCs.

a. Schematic showing endogenous tagging strategy to introduce the RITE system at the 3' end of the *Nup221* gene. Translocation of Cre-EBD to the nucleus following treatment with β-estradiol results in excision between loxP sites, removing the original 3xHA/GFP tag while bringing the 3xMyc/RFP tag into frame. **b.** Representative images of *P. berghei* parasites at 0 hours post, 10 hours post, and 20 hours post induction with β-estradiol. HA signal (Scale bars 2 µm, Image depth in µm indicated. White arrows indicate areas of colocalization between HA and Myc. **c.** Ratio Nup221-HA/Nup221-Myc foci in 0 hours-, 10 hours- and 20 hours post induction with β-estradiol. Green bars indicate number of foci that had both HA and Myc signal. **d.** Amount of HA or Myc signal found around the CP in 10 hour- and 20 hour post induction parasites determined by counting foci around the CP. Green bars indicate foci containing both HA and Myc signal.

371 **Methods:**

372 **Parasite maintenance**

373 *P. berghei* ANKA clone 2.34 and derivatives were maintained in Swiss Webster mice
374 (Charles River). All experiments involving rodents were reviewed and approved by the Iowa State
375 University Institutional Animal Care and Use Committee.

376 **Genetic modification of *Plasmodium berghei***

377 Plasmid cloning was carried out using NEBuilder HIFI DNA assembly (NEB). Primer
378 sequences are given in Table 1. To generate a smHA [54] fusion at the endogenous C terminus of
379 *P. berghei* Nup138 the smHA coding sequence was amplified from plasmid
380 pCAG_smFP_HA(Addgene #59759) using primers P4121/4122 and inserted between
381 BamHI/BsiWI immediately downstream of the *Pbnup138* homology region in the plasmid
382 pLIS0654 [17] resulting in the plasmid pSA026. To generate a smHA fusion at the endogenous C
383 terminus of *P. berghei* Nup313, a homology region corresponding to the 3' coding sequence of
384 *Pbnup313* up to but not including the stop codon was amplified with primers P4140/4126 from
385 *P. berghei* genomic DNA and inserted between AvrII/BamHI in pSA026, replacing the *Pbnup138*
386 homology region and resulting in the plasmid pSA028.

387 To generate parasites expressing Cre-EBD with the RITE cassette fused to the endogenous
388 C terminus of *P. berghei* Nup221, the Cre-EBD coding sequence was amplified from the plasmid
389 pTWO40 [55] (Addgene #64769) and the RITE cassette was amplified from the plasmid pKV016,
390 which includes a 3xHA-GFP fusion in the pre-excised state and a 3xMYC-mRFP fusion in the post-
391 excised state [56] (Addgene #64767). These sequences were assembled together with a
392 *Pbnup221* homology region [17], placing Cre-EBD under the control of *P. berghei* EF1 alpha
393 promoter and the hDHFR selectable marker under the control of the *P. berghei* EF1 delta
394 promoter and positioning the hDHFR cassette between the two loxP-containing RITE tags to
395 facilitate marker removed upon excision. The mRFP sequence in the post-excision RITE fusion
396 was subsequently replaced with mRuby3 to yield the final plasmid pL857.

397 Plasmids pSA026, pSA028 and pL857 were linearized within the *Pbnup138*, *Pbnup313 or*
398 *Pbnup221* homology region using HindIII, PacI or ScaI, respectively, and transfected into *P.*
399 *berghei* as described [57]. Transfected parasites were injected into naïve mice and selected with
400 0.07 mg/ml pyrimethamine provided *ad libitum* in drinking water beginning 24 hours post-
401 transfection. Parasites were genotyped to confirm integration at *Pbnup138*, *Pbnup313* or
402 *Pbnup221* using PCR strategies described in Supplementary Figures 2 and 4.

403 **Live imaging and immunofluorescence assays**

404 For live imaging of parasites at regular intervals throughout the experiment, 100µl
405 parasite culture was spun down and resuspended in PBS containing 1µg/ml Hoechst 33342 to
406 stain nuclei. Following a brief incubation at 37°C, parasites were imaged with a 63x objective on
407 an Axio Observer 7 equipped with an Axiocam 702 mono camera and Zen 2.6 Pro software (Zeiss)
408 using the same exposure times for all images across sample groups and experimental
409 replicates.For immunofluorescence assays on unexpanded cells, thin blood smears were air dried
410 and fixed in ice-cold methanol/acetone (50:50) (for detection of smHA tagged Nup138, Nup313
411 or for detection of Cre). Fixed slides were blocked with Rockland blocking buffer (Rockland) and
412 probed with the primary and secondary antibodies indicated below. ,Slides were mounted in
413 Fluoromount-G with DAPI (Invitrogen).

414 **Ultrastructure expansion microscopy**

415 Ultrastructure expansion microscopy was performed as previously described on fixed
416 samples. Briefly, parasites were fixed in 4% PFA/PBS supplemented with 0.0075% glutaraldehyde
417 by the lab of Dr. Josh Beck at Iowa State University and were sent to the lab of Dr. Sabrina Absalon
418 at Indiana University School of Medicine. 12 mm round coverslips (Fisher Cat. No. NC1129240)
419 were treated with poly-D-lysine for 1 hour at 37 °C, washed three times with MilliQ water, and
420 placed in the wells of a 24-well dish. Fixed samples were resuspended at roughly 1.0 % hematocrit
421 in 1xPBS and 500 µL of parasite sample was added to the wells containing the coated coverslips
422 for 30 minutes at 37 °C. Following parasites settling, coverslips were washed 3 times in 1xPBS
423 before treating with 500 µL 1.4% v/v formaldehyde/2% v/v acylamide (FA/AA) in PBS. Samples

424 were incubated overnight at 37 °C. Gelation, denaturation, staining, and expansion of the gels
425 were performed as previously described [24]. Stained gels were imaged using a Zeiss LSM900
426 AxioObserver with an Airyscan 2 detector. Images were taken using a 63x Plan-Apochromat
427 objective lens with a numerical aperature of 1.4.

428 **RITE experiment setup**

429 Asynchronous Nup221::RITE *P. berghei* parasites were collected and allowed to develop
430 overnight in vitro into terminal schizonts. Schizonts were magnetically purified on a MACS LD
431 column (Miltenyi Biotec) and IV injected into naïve mice to establish a synchronous infection.
432 Infections were allowed to develop for three intraerythrocytic developmental cycles (IDCs) to
433 increase parasitemia, then collected at 72 hpi when parasites were predominantly ring stage and
434 passed through a MACS LD column to remove any trophozoites or schizonts by collecting the flow
435 through.

436 These synchronized ring-stage parasites were used to establish in vitro cultures in
437 complete RPMI containing 200nM β-estradiol or DMSO (vehicle control). Parasites were collected
438 every two hours for live imaging and genomic DNA isolation. After 24 hours, parasites were
439 washed to remove β-estradiol or DMSO and IV injected into naïve mice to monitor Nup turnover
440 in subsequent IDCs. Mice were not provided with pyrimethamine to avoid killing parasites that
441 had undergone excision, which also removes the hDHFR selection marker.

442 **Antibodies and stains**

443 The following antibodies were used for widefield IFA analysis: rabbit polyclonal anti-HA
444 (1:500, Thermofisher SG77), rabbit anti-Cre polyclonal (1:500, Abcam ab190177). The following
445 antibodies were used for the preparation of stained gels for expansion microscopy: Rat anti-HA
446 (3F10, 1:25, Roche 12158167001), Mouse IgG1 anti-alpha Tubulin Clone B-5-1-2 (1:500,
447 ThermoFisher 32-2500), Rabbit anti-Myc polyclonal (1:500, ThermoFisher 710007). Goat anti-
448 rabbit Alexa Fluor 594 (1:500, ThermoFisher A11012), Goat anti-rat Alexa Fluor 488 (1:500,
449 ThermoFisher A1106), Goat anti-mouse IgG(H+L) Alexa Fluor 555 (1:500, ThermoFisher A21422),

450 and Goat anti-rabbit Alexa Fluor 555 (1:500, ThermoFisher A32732) were used as secondary
451 antibodies. NHS Ester Alexa Fluor 405 in DMSO (8 µg/mL, ThermoFisher A30000) was used to
452 stain proteins and SYTOX™ Deep Red (1 µM, ThermoFisher S11380) was used as a DNA stain.

453 **Image analysis**

454 All image analysis was done using 3D Airyscan processing at moderate filter strength on
455 Zen Blue Version 3.1 (Zeiss, Oberkochen, Germany). Images shown in this manuscript are
456 maximum intensity projections of between 5 and 60 z-slices of the entire image, with the number
457 indicated as the total Z-depth of the image (Z depth = 0.13 µm * number of slices taken for
458 projection)

459 **Statistical analysis**

460 Graphical data and statistical analysis was performed on Graphpad Prism version 9.0.

461 **Acknowledgements**

462 We thank The Company of Biologists Travelling Fellowship grant JCSTF2202676 (S.V.A)
463 for initial travel funding to begin this project. This work was supported by NIH grant AI139579
464 (G.R.M. and J.R.B.) and was made possible by an award from the Indiana University School of
465 Medicine (S.A., BRG award #2286272). The content is solely the responsibility of the authors
466 and does not necessarily represent the official views of the Indiana University School of
467 Medicine.

468 **Table S1. Sequences of primers used in this study.**

Name	Sequence
P4121	GTTATTCTCACGAGCTTAGAAATATGAAGGGATCCATGTACCCTTATGATGTGCCCGATTATGC
P4122	GATAGCCAGCGTAGTCCGGGACGTCGTACGGGTAGCCACCCTTGTAGAGTTCGTC
P4140	GACGATAAAAATGAAAATACAAATCCTAGGGAAATTGAAATCGCTTGCACATATTTGAATC
P4126	CATCATAAGGGTACATGGATCCGTTTATGACATTTTGGCTAGTG
P5	GGAAAAAGCTTAACATTTAACTCTTCATTTTTTAAAACGAGCAC
P6	CCGGGACGTCGTACGGG

P7	CTTAGCCCATGCGAATGCATACTATTAGAAC
P8	GTCCATTAACGTCGCCATCCAACTCC
P3922	TTTAAATGATACAAAACACAGACG
P3915	ATACTAGTAGCGTAATCTGGAACG
P3888	TCAATGATTCATAAATAGTTGGACTTG
P3659	ATCAACAAATTATAAATGACAGAAC
P3004	AAAAGATCTATGGTTGGTTCGCTAAACTG
P3005	AAACAATTGTTAATCATTCTTCTCATATAC
P3491	GATAAATTCTCGAGCCCGGGTATCGATTATTTAGAGAATC
P3492	TCTTTACCTCCGCCGGATCCAATATTTTTAATAACATTTC
P4046	TTCCATGACCACCTTCATACGC
P3921	CGCATGAACTCCTTGATGACG

Table S2: Plasmids used in this study.

Genotype	Plasmid Name
nup138::smHA	pSA026
nup313::smHA	pSA028
nup221::RITE	pL857

Author Contributions:

Conceptualization: J.B., S.V.A., G.R.M., J.R.B., and S.A.; **Methodology:** J.B., S.V.A., G.R.M., J.R.B., and S.A.; **Investigation:** J.B., S.V.A., and T.H.; **Data Analysis:** J.B. **Writing – Original Draft:** J.B.; **Writing – Review and Editing:** J.B., S.V.A., T.H., G.R.M., J.R.B., and S.A; **Funding Acquisition:** S.V.A., G.R.M., J.R.B., and S.A.; **Supervision:** G.R.M., J.R.B. and S.A.

References:

1. Lin, D.H. and A. Hoelz, *The Structure of the Nuclear Pore Complex (An Update).* Annu Rev Biochem, 2019. **88**: p. 725-783.

481 2. Hoelz, A., E.W. Debler, and G. Blobel, *The Structure of the Nuclear Pore Complex.* Annual Review
482 of Biochemistry, 2011. **80**(1): p. 613-643.
483 3. Grossman, E., O. Medalia, and M. Zwerger, *Functional Architecture of the Nuclear Pore Complex.*
484 Annual Review of Biophysics, 2012. **41**(1): p. 557-584.
485 4. Ori, A., et al., *Cell type-specific nuclear pores: a case in point for context-dependent stoichiometry*
486 *of molecular machines.* Mol Syst Biol, 2013. **9**: p. 648.
487 5. Otsuka, S. and J. Ellenberg, *Mechanisms of nuclear pore complex assembly – two different ways*
488 *of building one molecular machine.* FEBS Letters, 2018. **592**(4): p. 475-488.
489 6. Courjol, F., et al., *Characterization of a nuclear pore protein sheds light on the roles and*
490 *composition of the Toxoplasma gondii nuclear pore complex.* Cell Mol Life Sci, 2017. **74**(11): p.
491 2107-2125.
492 7. Degrasse, J.A. and D. Devos, *A functional proteomic study of the Trypanosoma brucei nuclear*
493 *pore complex: an informatic strategy.* Methods Mol Biol, 2010. **673**: p. 231-8.
494 8. Beck, M. and E. Hurt, *The nuclear pore complex: understanding its function through structural*
495 *insight.* Nature Reviews Molecular Cell Biology, 2017. **18**(2): p. 73-89.
496 9. Devos, D., et al., *Simple fold composition and modular architecture of the nuclear pore complex.*
497 Proc Natl Acad Sci U S A, 2006. **103**(7): p. 2172-7.
498 10. Strawn, L.A., et al., *Minimal nuclear pore complexes define FG repeat domains essential for*
499 *transport.* Nature Cell Biology, 2004. **6**(3): p. 197-206.
500 11. Dey, G., et al., *Closed mitosis requires local disassembly of the nuclear envelope.* Nature, 2020.
501 **585**(7823): p. 119-123.
502 12. Lénárt, P., et al., *Nuclear envelope breakdown in starfish oocytes proceeds by partial NPC*
503 *disassembly followed by a rapidly spreading fenestration of nuclear membranes.* J Cell Biol, 2003.
504 **160**(7): p. 1055-68.
505 13. Gerald, N., B. Mahajan, and S. Kumar, *Mitosis in the human malaria parasite Plasmodium*
506 *falciparum.* Eukaryotic cell, 2011. **10**(4): p. 474-482.
507 14. Neumann, N., D. Lundin, and A.M. Poole, *Comparative genomic evidence for a complete nuclear*
508 *pore complex in the last eukaryotic common ancestor.* PLoS One, 2010. **5**(10): p. e13241.
509 15. Kehrer, J., et al., *Nuclear Pore Complex Components in the Malaria Parasite Plasmodium berghei.*
510 Scientific Reports, 2018. **8**(1): p. 11249.
511 16. Dahan-Pasternak, N., et al., *PfSec13 is an unusual chromatin-associated nucleoporin of*
512 *Plasmodium falciparum that is essential for parasite proliferation in human erythrocytes.* Journal
513 of Cell Science, 2013. **126**(14): p. 3055-3069.
514 17. Ambekar Sushma, V., R. Beck Josh, and R. Mair Gunnar, *TurboID Identification of Evolutionarily*
515 *Divergent Components of the Nuclear Pore Complex in the Malaria Model Plasmodium berghei.*
516 mBio, 2022. **13**(5): p. e01815-22.
517 18. Bertiaux, E., et al., *Expansion microscopy provides new insights into the cytoskeleton of malaria*
518 *parasites including the conservation of a conoid.* PLoS Biol, 2021. **19**(3): p. e3001020.
519 19. Colombi, P., et al., *The transmission of nuclear pore complexes to daughter cells requires a*
520 *cytoplasmic pool of Nsp1.* Journal of Cell Biology, 2013. **203**(2): p. 215-232.
521 20. Doye, V., R. Wepf, and E.C. Hurt, *A novel nuclear pore protein Nup133p with distinct roles in*
522 *poly(A)+ RNA transport and nuclear pore distribution.* The EMBO Journal, 1994. **13**(24): p. 6062-
523 6075.
524 21. Weiner, A., et al., *3D nuclear architecture reveals coupled cell cycle dynamics of chromatin and*
525 *nuclear pores in the malaria parasite Plasmodium falciparum.* Cellular Microbiology, 2011. **13**(7):
526 p. 967-977.

527 22. Winey, M., et al., *Nuclear Pore Complex Number and Distribution throughout theSaccharomyces*
528 *cerevisiae Cell Cycle by Three-Dimensional Reconstruction from Electron Micrographs of Nuclear*
529 *Envelopes.* Molecular Biology of the Cell, 1997. **8**(11): p. 2119-2132.
530 23. Caroline, S.S., et al., *An extended DNA-free intranuclear compartment organizes centrosome*
531 *microtubules in malaria parasites.* Life Science Alliance, 2021. **4**(11): p. e202101199.
532 24. Liffner, B. and S. Absalon *Expansion Microscopy Reveals Plasmodium falciparum Blood-Stage*
533 *Parasites Undergo Anaphase with A Chromatin Bridge in the Absence of Mini-Chromosome*
534 *Maintenance Complex Binding Protein*. Microorganisms, 2021. **9**, DOI:
535 10.3390/microorganisms9112306.
536 25. Liffner, B., et al., *Atlas of Plasmodium falciparum intraerythrocytic development using expansion*
537 *microscopy*. 2023, eLife Sciences Publications, Ltd.
538 26. Gambarotto, D., et al., *Imaging cellular ultrastructures using expansion microscopy (U-ExM).* Nat
539 Methods, 2019. **16**(1): p. 71-74.
540 27. Toyama, B.H., et al., *Visualization of long-lived proteins reveals age mosaicism within nuclei of*
541 *postmitotic cells.* Journal of Cell Biology, 2018. **218**(2): p. 433-444.
542 28. Verzijlbergen, K.F., et al., *Recombination-induced tag exchange to track old and new proteins.*
543 Proceedings of the National Academy of Sciences, 2010. **107**(1): p. 64-68.
544 29. Hinterndorfer, K., et al., *Ultrastructure expansion microscopy reveals the cellular architecture of*
545 *budding and fission yeast.* Journal of Cell Science, 2022. **135**(24): p. jcs260240.
546 30. Arnot, D.E., E. Ronander, and D.C. Bengtsson, *The progression of the intra-erythrocytic cell cycle*
547 *of Plasmodium falciparum and the role of the centriolar plaques in asynchronous mitotic division*
548 *during schizogony.* Int J Parasitol, 2011. **41**(1): p. 71-80.
549 31. Simon, C.S., et al., *An extended DNA-free intranuclear compartment organizes centrosome*
550 *microtubules in malaria parasites.* Life Sci Alliance, 2021. **4**(11).
551 32. Allegretti, M., et al., *In-cell architecture of the nuclear pore and snapshots of its turnover.* Nature,
552 2020. **586**(7831): p. 796-800.
553 33. Lee, C.-W., et al., *Selective autophagy degrades nuclear pore complexes.* Nature Cell Biology,
554 2020. **22**(2): p. 159-166.
555 34. Tomioka, Y., et al., *TORC1 inactivation stimulates autophagy of nucleoporin and nuclear pore*
556 *complexes.* J Cell Biol, 2020. **219**(7).
557 35. Fernandes, P., et al., *The dimerisable Cre recombinase allows conditional genome editing in the*
558 *mosquito stages of Plasmodium berghei.* PLoS One, 2020. **15**(10): p. e0236616.
559 36. Kent, R.S., et al., *Inducible developmental reprogramming redefines commitment to sexual*
560 *development in the malaria parasite Plasmodium berghei.* Nat Microbiol, 2018. **3**(11): p. 1206-
561 1213.
562 37. Ferreira, J.L., et al., *Variable microtubule architecture in the malaria parasite.* Nat Commun,
563 2023. **14**(1): p. 1216.
564 38. Chial, H.J., et al., *Saccharomyces cerevisiae Ndc1p is a shared component of nuclear pore*
565 *complexes and spindle pole bodies.* J Cell Biol, 1998. **143**(7): p. 1789-800.
566 39. Jaspersen, S.L. and S. Ghosh, *Nuclear envelope insertion of spindle pole bodies and nuclear pore*
567 *complexes.* Nucleus, 2012. **3**(3): p. 226-36.
568 40. Gomar-Alba, M. and M. Mendoza, *Modulation of Cell Identity by Modification of Nuclear Pore*
569 *Complexes.* Frontiers in Genetics, 2020. **10**.
570 41. Kane, M., et al., *Nuclear pore heterogeneity influences HIV-1 infection and the antiviral activity of*
571 *MX2.* eLife, 2018. **7**: p. e35738.
572 42. Hinshaw, J.E. and R.A. Milligan, *Nuclear pore complexes exceeding eightfold rotational symmetry.*
573 Journal of Structural Biology, 2003. **141**(3): p. 259-268.

574 43. Unwin, P.N. and R.A. Milligan, *A large particle associated with the perimeter of the nuclear pore*
575 *complex.* Journal of Cell Biology, 1982. **93**(1): p. 63-75.
576 44. Pulianmackal, A.J., et al., *Misregulation of Nucleoporins 98 and 96 leads to defects in protein*
577 *synthesis that promote hallmarks of tumorigenesis.* Dis Model Mech, 2022. **15**(3).
578 45. Ferreira, J., J.H. Stear, and H. Saumweber, *Nucleoporins NPP-10, NPP-13 and NPP-20 are required*
579 *for HCP-4 nuclear import to establish correct centromere assembly.* J Cell Sci, 2017. **130**(5): p.
580 963-974.
581 46. Wu, X., et al., *Disruption of the FG nucleoporin NUP98 causes selective changes in nuclear pore*
582 *complex stoichiometry and function.* Proceedings of the National Academy of Sciences, 2001.
583 **98**(6): p. 3191-3196.
584 47. Powers, M.A., et al., *The vertebrate GLFG nucleoporin, Nup98, is an essential component of*
585 *multiple RNA export pathways.* J Cell Biol, 1997. **136**(2): p. 241-50.
586 48. Gomes, A.R., et al., *A genome-scale vector resource enables high-throughput reverse genetic*
587 *screening in a malaria parasite.* Cell Host Microbe, 2015. **17**(3): p. 404-413.
588 49. Bushell, E., et al., *Functional Profiling of a Plasmodium Genome Reveals an Abundance of*
589 *Essential Genes.* Cell, 2017. **170**(2): p. 260-272.e8.
590 50. Zhang, M., et al., *Uncovering the essential genes of the human malaria parasite Plasmodium*
591 *falciparum by saturation mutagenesis.* Science, 2018. **360**(6388).
592 51. Dey, G. and B. Baum, *Nuclear envelope remodelling during mitosis.* Curr Opin Cell Biol, 2021. **70**:
593 p. 67-74.
594 52. Linder, M.I., et al., *Mitotic Disassembly of Nuclear Pore Complexes Involves CDK1- and PLK1-*
595 *Mediated Phosphorylation of Key Interconnecting Nucleoporins.* Dev Cell, 2017. **43**(2): p. 141-
596 156.e7.
597 53. Kutay, U., R. Jühlen, and W. Antonin, *Mitotic disassembly and reassembly of nuclear pore*
598 *complexes.* Trends in Cell Biology, 2021. **31**(12): p. 1019-1033.
599 54. Viswanathan, S., et al., *High-performance probes for light and electron microscopy.* Nat Methods,
600 2015. **12**(6): p. 568-76.
601 55. Terweij, M., et al., *Recombination-induced tag exchange (RITE) cassette series to monitor protein*
602 *dynamics in Saccharomyces cerevisiae.* G3 (Bethesda), 2013. **3**(8): p. 1261-72.
603 56. Menendez-Benito, V., et al., *Spatiotemporal analysis of organelle and macromolecular complex*
604 *inheritance.* Proc Natl Acad Sci U S A, 2013. **110**(1): p. 175-80.
605 57. Hussain, T., et al., *The PTEX Pore Component EXP2 Is Important for Intrahepatic Development*
606 *during the Plasmodium Liver Stage.* mBio, 2022. **13**(6): p. e0309622.

607

608

609

610

611

612 **Supplemental Figures:**

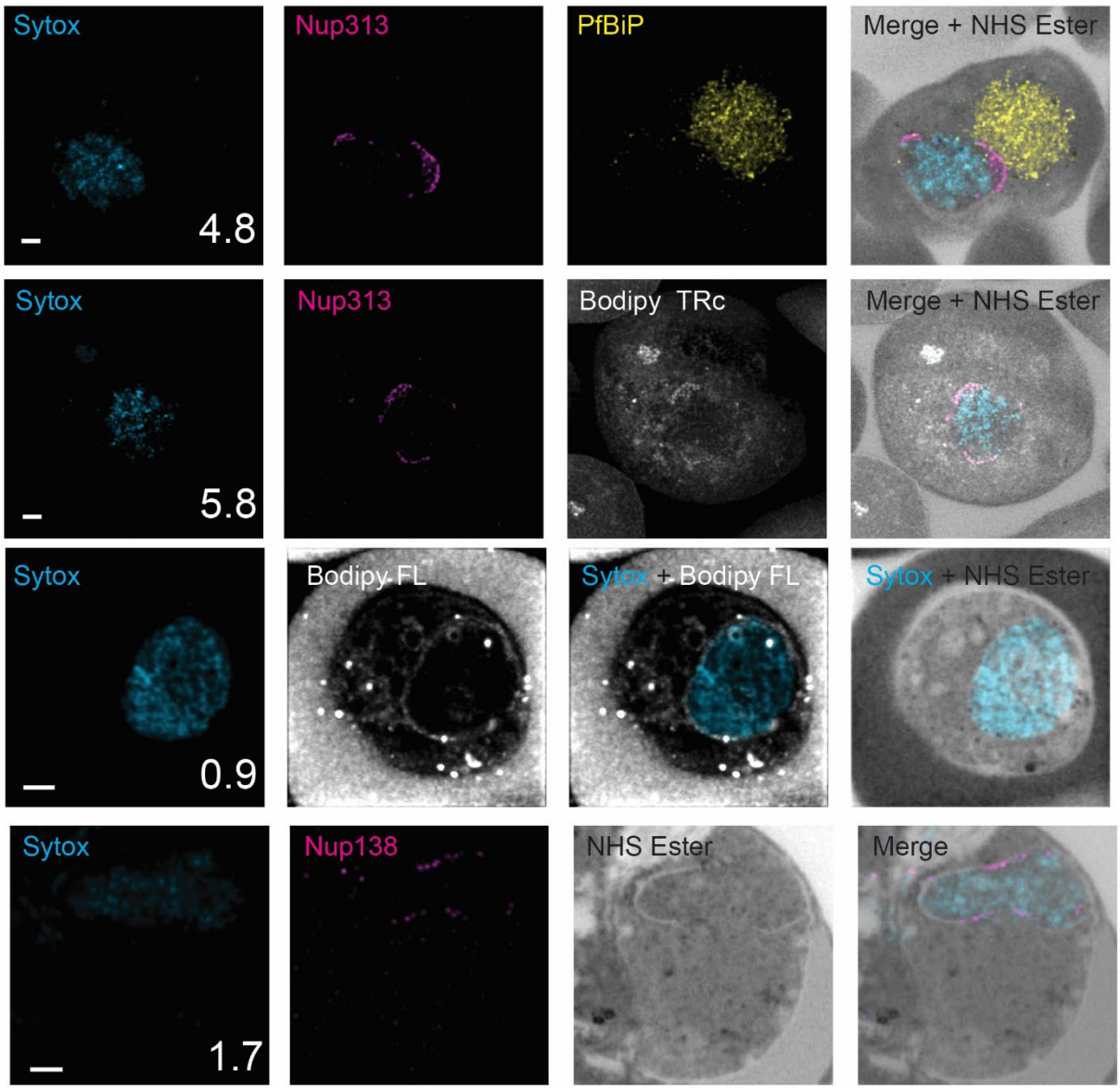

613

614 **Supplemental figure 1: Nuclear envelope visualization in *P. berghei*.** Staining with the
615 endoplasmic reticulum protein PfBip (top image, yellow), Bodipy TR ceramide and Bodipy FL
616 ceramide to stain for membranes (middle images, white), and differences in NHS ester staining
617 (grayscale) to visualize the nuclear envelope. Magenta indicates Nup138 or Nup313, scale bars 2
618 µm, image depth in µm indicated.

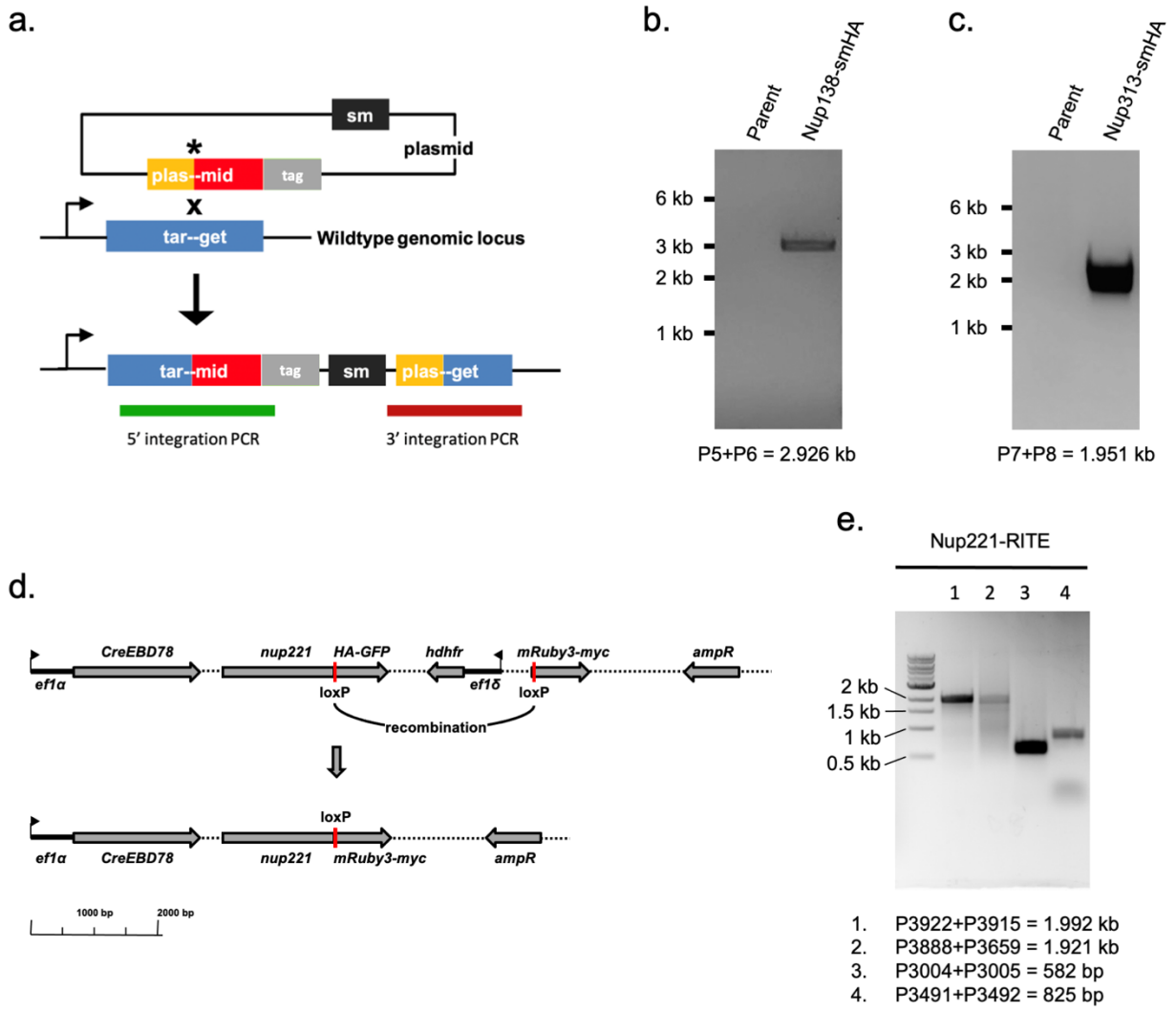

Supplemental figure 2: Genotyping of Nup138, Nup313 and Nup221 endogenously tagged parasite lines. a. Schematic of general strategy for integration into the endogenous Nup138, Nup313 and Nup221 loci to generate C-terminal tag fusions. The plasmid is linearized with the homology flank targeting each gene (yellow/red box). Following transfection, homologous recombination into the target locus (blue box) results in fusion of the tag to the 3' end of the gene. Green and red lines show integration PCR products diagnostic for the successful integration. sm, selectable marker. **b,c.** 5' integration PCRs for Nup138-smHA and Nup313-smHA parasites. **d.** Schematic of the plasmid used to generate the Nup221-RITE parasites. Cre-mediated recombination between loxP sequences removes the 3xHA-GFP tag and hDHFR selection marker and brings the mRuby3-3xMyc tag into frame. **e.** Integration PCRs for the Nup221-RITE parasites.

630 Reactions 1 and 2 are diagnostic for successful 5’ and 3’ integration, respectively. Reactions 3 and
631 4 are controls amplifying an internal portion of the plasmid and an unrelated genomic locus,
632 respectively.

633

634

635

636

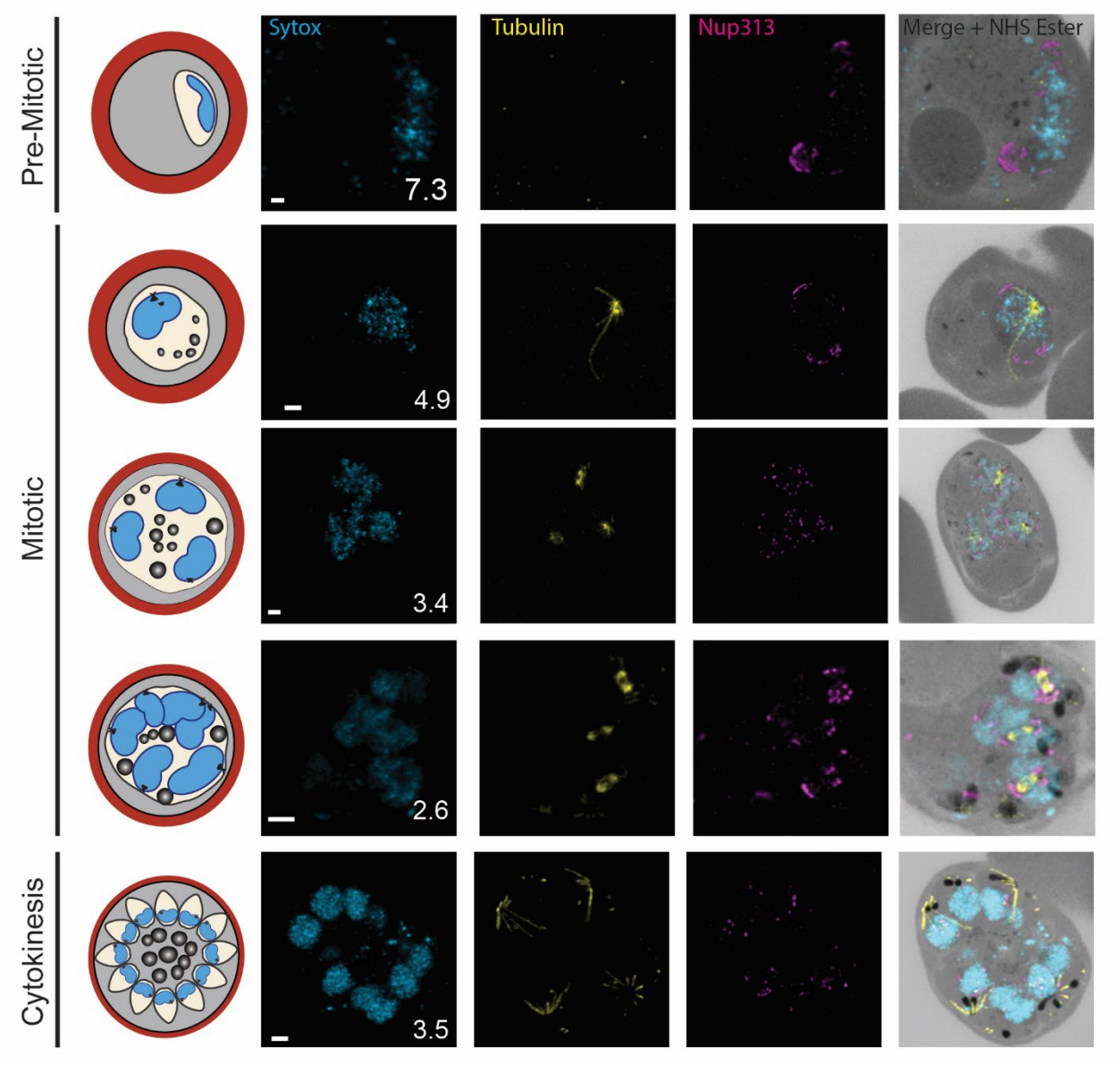

Supplemental figure 3: Nup313 through the P. berghei blood stage life cycle. U-ExM images showing Nup313 at early stages and Nup138 through the life cycle of *P. berghei*. DNA shown in blue, microtubules shown in yellow, Nup313 shown in magenta, protein density shown in grayscale. Scale bars 2 µm, image depth in µm indicated.

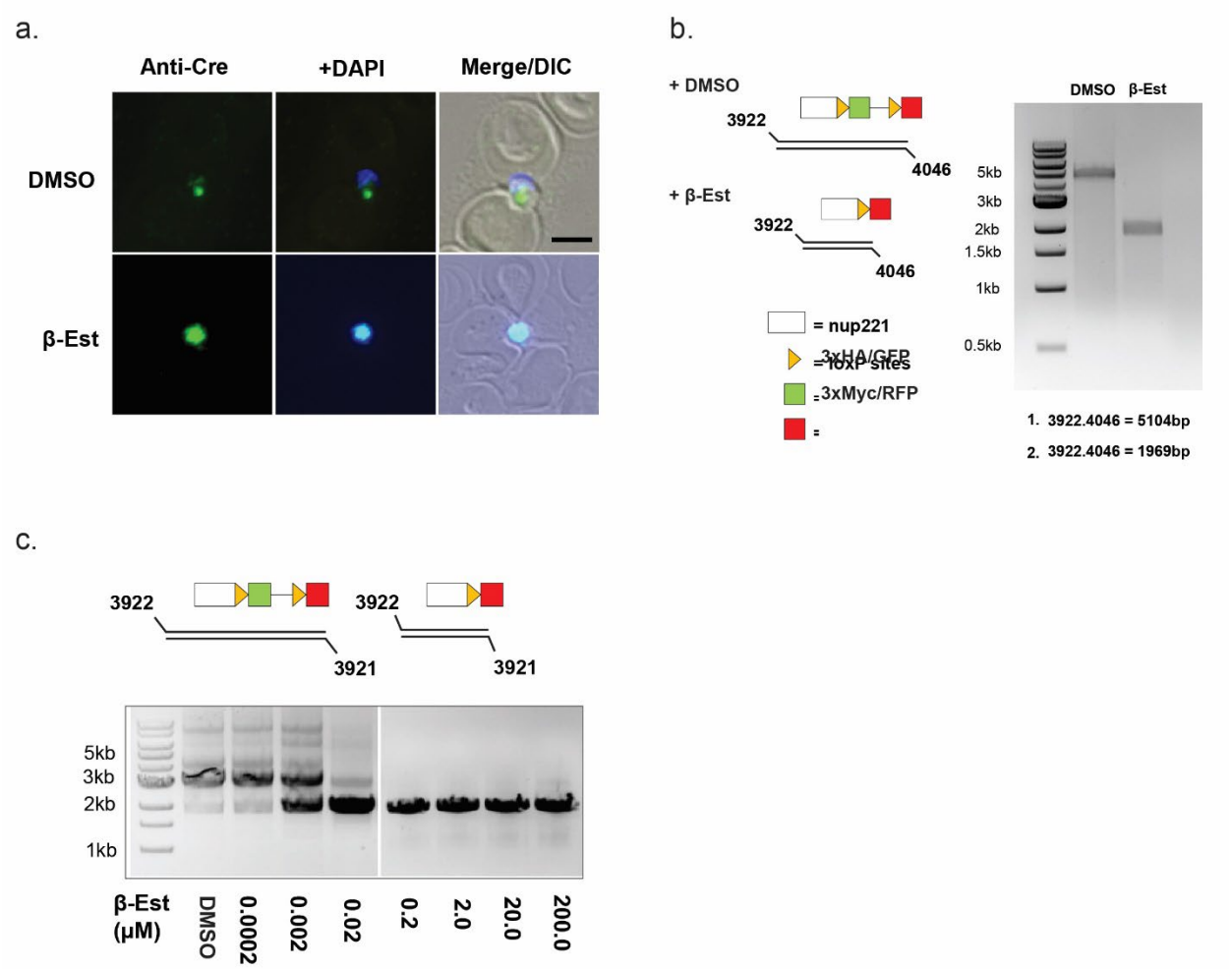

Supplemental figure 4: Cre-EBD enables inducible genomic excision in *P. berghei.* a. Immunofluorescence of Cre-EBD expressing *P. berghei* parasites. The addition of β-estradiol to the parasites induces the Cre-EBD to translocate to the nucleus. Scale bar 2 µm. **b.** PCR showing genome shift upon addition of β-estradiol, inducing a tag switch. Primers used are indicated in the diagrams and expected length of PCR products are listed. **c.** PCR showing concentration dependence of the RITE system tested from 0.0002 µM to 200 µM β-estradiol. 2 nM β-estradiol is sufficient to induce a partial tag switch, while 200 nM β-estradiol was sufficient to induce a total tag switch after 2 hours of treatment. PCR primers used are listed in the diagram.

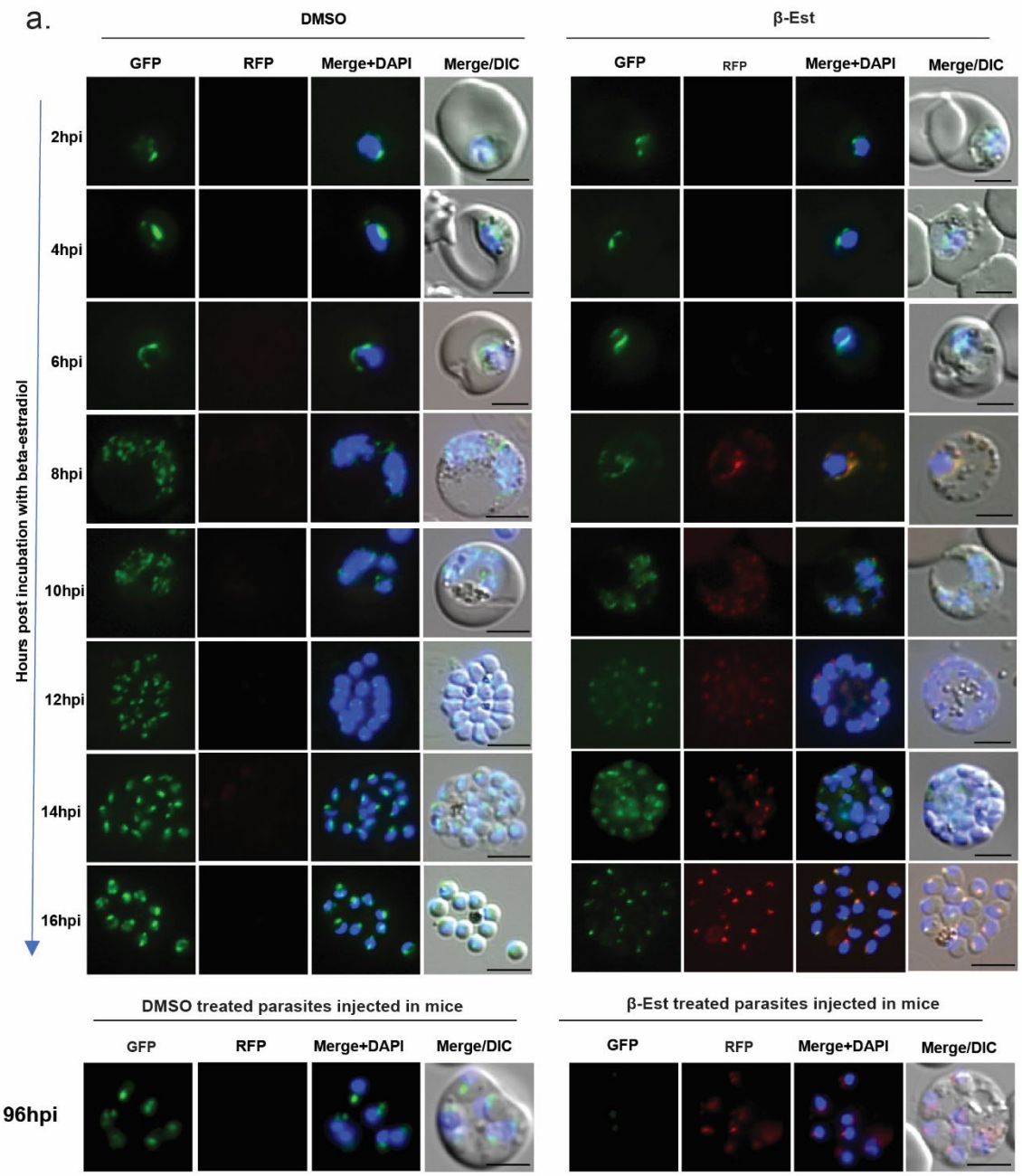
a.
DMSO
β-Est
GFP
RFP
Merge+DAPI
Merge/DIC
Hours post incubation with beta-estradiol
2hpi
4hpi
6hpi
8hpi
10hpi
12hpi
14hpi
16hpi
DMSO treated parasites injected in mice
β-Est treated parasites injected in mice
96hpi

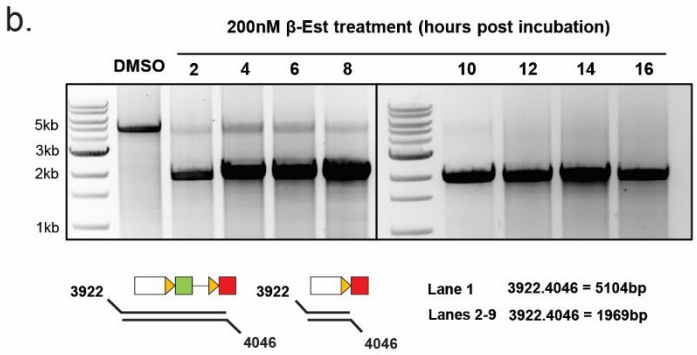
b.
200nM β-Est treatment (hours post incubation)
DMSO
2
4
6
8
10
12
14
16
5kb
3kb
2kb
1kb
3922
4046
3922
4046
Lane 1 3922.4046 = 5104bp
Lanes 2-9 3922.4046 = 1969bp

655

656 **Supplemental figure 5: Time course of the RITE system in *P. berghei* of Nup221::RITE. a.** Live
657 imaging of Nup221::RITE parasites showing control or β-estradiol treated parasites during 16
658 hours of treatment, samples taken every 2 hours. In addition, parasites were cultured an
659 additional 80 hours, where β-estradiol treated parasites only showed RFP signal and control
660 parasites still only showed GFP signal. Scale bars 2 µm. **b.** PCR gel showing the efficiency of Cre-
661 EBD system over 16 hours. PCR primers and expected band sizes are indicated in the diagram.

662

663

664

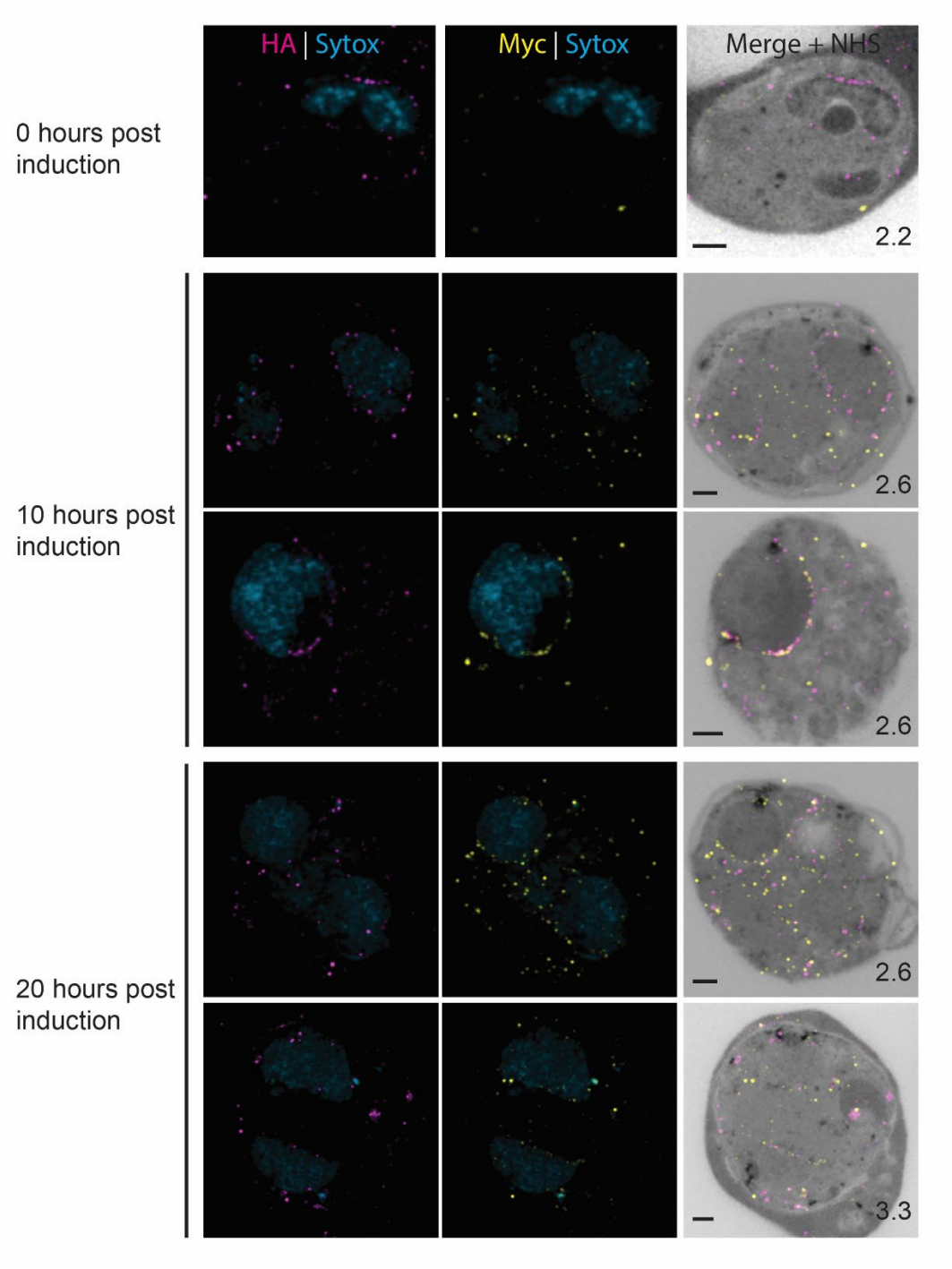

Supplemental figure 6: Uncropped images from Figure 4 showing Nup221::HA/GFP::Myc/RFP. U-ExM images showing the uncropped parasites in Figure 4. Age of the parasites is listed, HA signal represented in magenta, Myc signal represented in yellow, DNA represented in blue, protein density represented in grayscale. Scale bar 2 µm, image depth indicated in µm.